Energy transfer simulations with laterally varying heterogeneity: An explanation for Lg-wave blockage by the western Pyrenees

Christoph Sens-Schönfelder, Ludovic Margerin, Michel Campillo

Universität Leipzig, CEREGE Aix-en-Provence, LGIT Grenoble

February 14 2010

Contents

Contents

Contents

Contents

Medium of Propagation

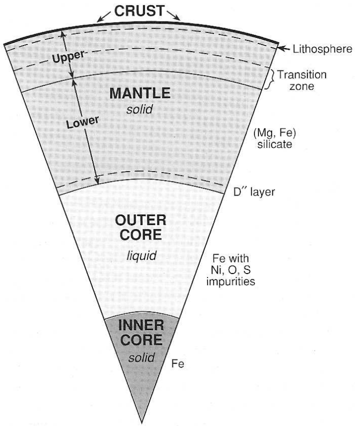

possible wave types:

- body waves
  - compressional waves
  - shear waves
- surface waves
  - Rayleigh waves
  - Love waves

Medium of Propagation

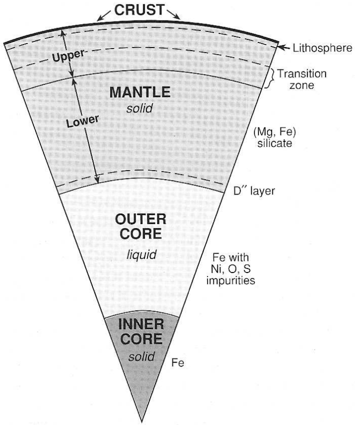

possible wave types:

- body waves
  - compressional waves
  - shear waves
- surface waves
  - Rayleigh waves
  - Love waves

Medium of Propagation

Medium of Propagation

geological processes ⇒ structural complexity

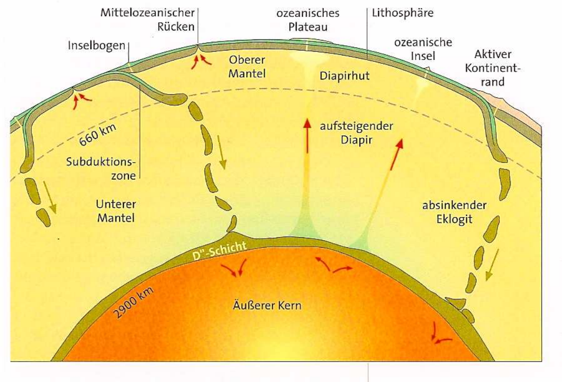

Medium of Propagation

large scale structure (e.g. interfaces, velocity gradients)

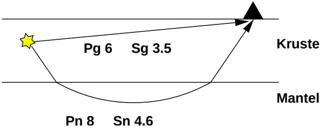

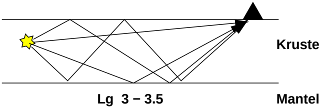

small scale heterogeneity

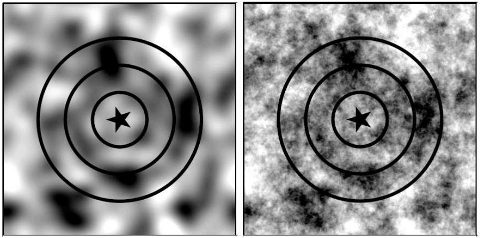

Przybilla et al. *JGR* 2006

Medium of Propagation

a real high frequency seismogram has a complex waveform

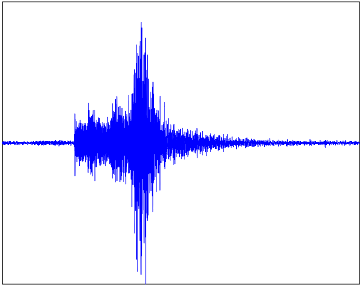

Medium of Propagation

a real high frequency seismogram has a complex waveform

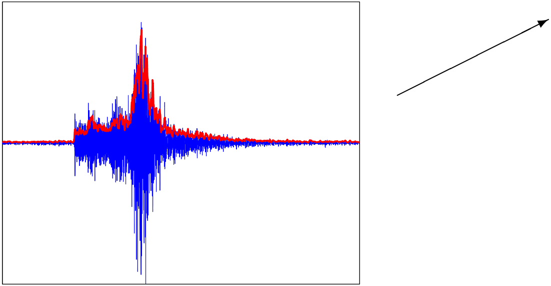

Amplitude

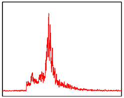

Medium of Propagation

a real high frequency seismogram has a complex waveform

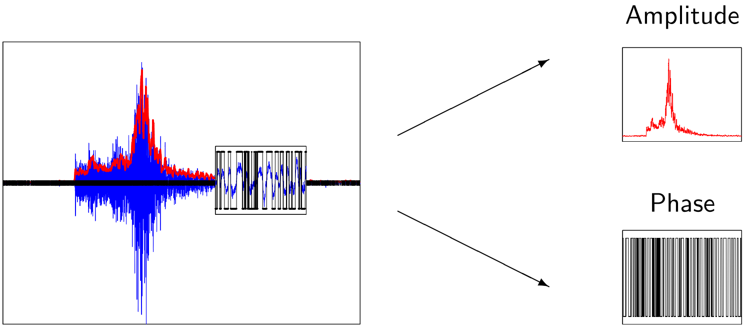

Medium of Propagation

seismogram envelope is basic information in this study

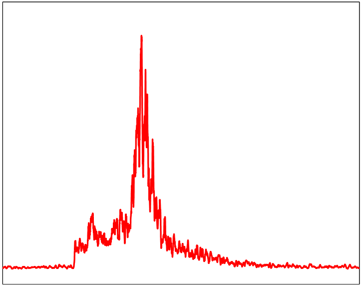

Earthquake Sources

anisotropic radiation of P and S waves from earthquakes

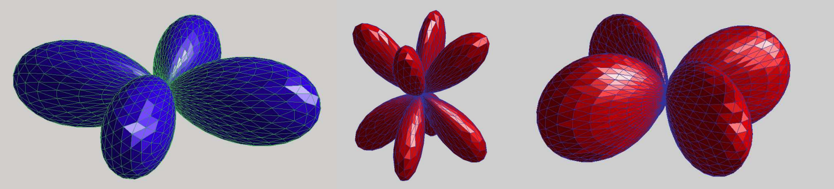

Earthquake Sources

anisotropic radiation of P and S waves from earthquakes

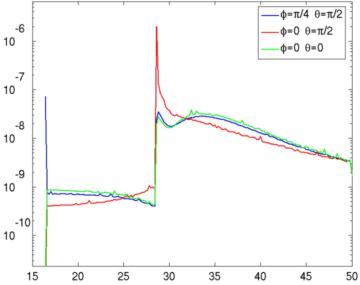

Previous Observations

Pyrenees: Chazalon et al. *GJI* 1993

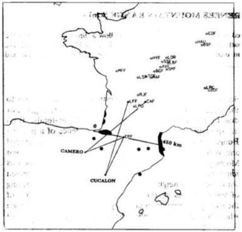

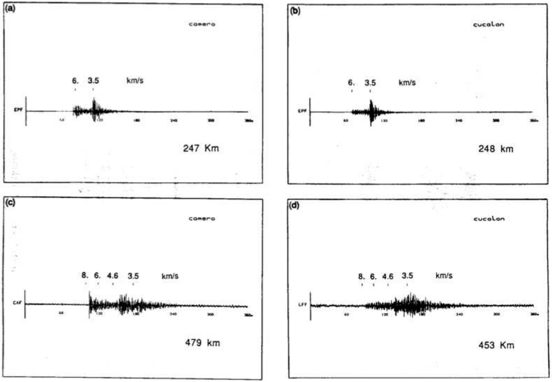

Previous Observations

Chazalon et al. *GJI* 1993

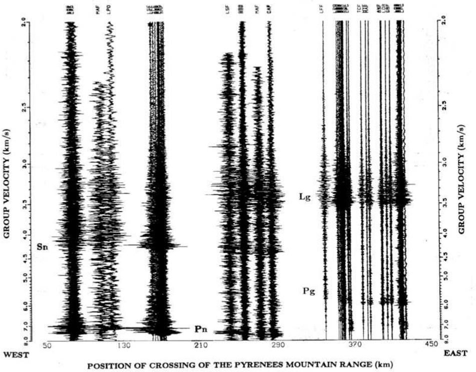

Previous Observations

Western Alps: Campillo et al. *JGR* 1993

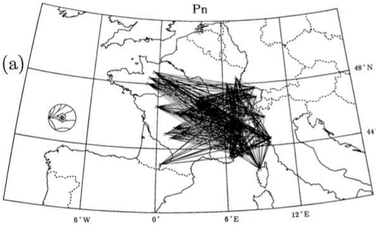

New Data

ray paths through the mountain range

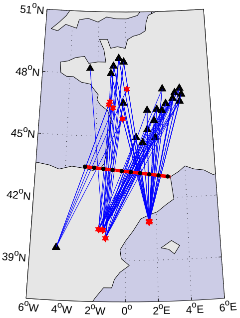

New Data

related traces

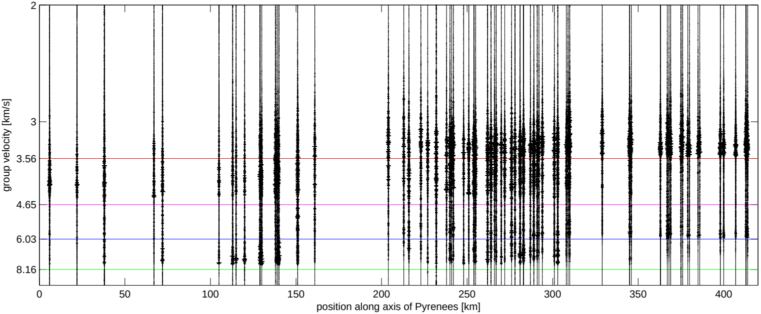

New Data

related traces

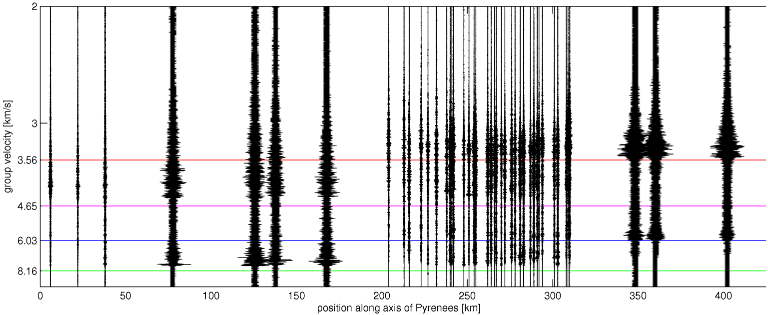

New Data

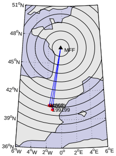
51°N
48°N
45°N
42°N
39°N
36°N
MFF
199199
6°W 4°W 2°W 0° 2°E 4°E 6°E

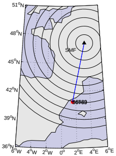
51°N
48°N
45°N
42°N
39°N
36°N
SMF
6°W 4°W 2°W 0° 2°E 4°E 6°E

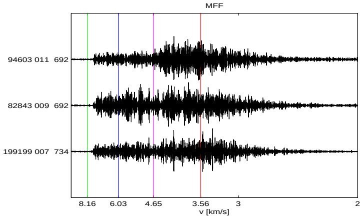
MFF
94603 011 692
82843 009 692
199199 007 734
8.16
6.03
4.65
3.56
3
2
v [km/s]

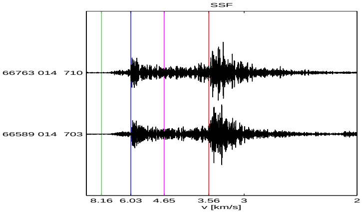
SSF
66763 014 710
66589 014 703
8.16
6.03
4.65
3.56
3
2
v [km/s]

New Data

averaged effect

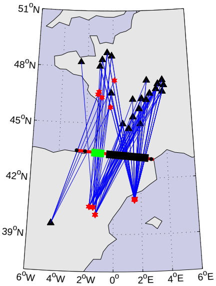

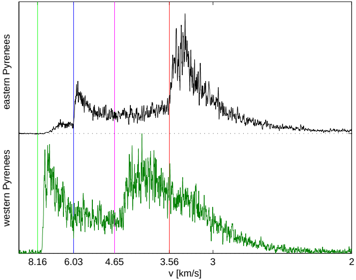

New Data

averaged effect

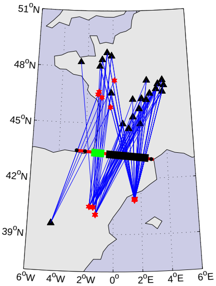

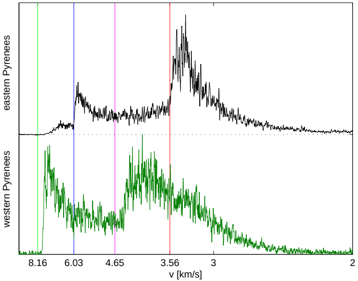

Lg blockage is an anomalous attenuation of waves that propagate in the curst compared to waves propagating below.

Structure of the Pyrenees

the geology is complicated

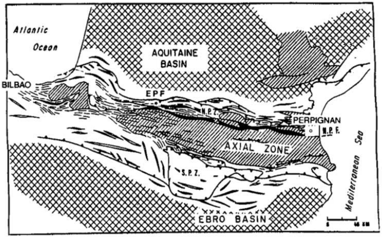

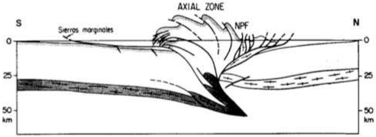

Chazalon et al. *GJI* 1993

Structure of the Pyrenees

in summary

- E-W oriented mountain range
- Jump in Moho depth from up to 50 km (Iberian plate) to about 30 - 35 km
- Subduction of Iberian lower crust only in the eastern part
- In the western Pyrenees: uplift of lower crustal block into the upper crust (distribution of earthquakes and tomography)

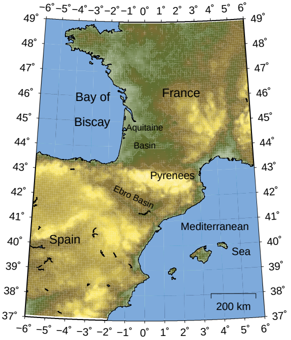

Large Scale Structure

effect of the jump in Moho depth

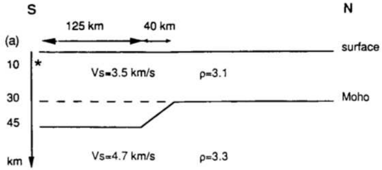

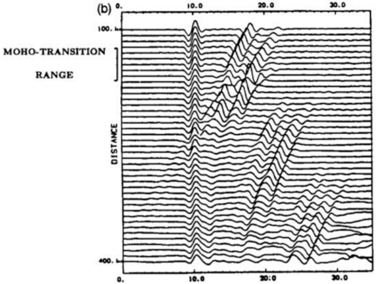

Chazalon et al. *GJI* 1993

Large Scale Structure

effect of uplifted lower crust bodies and Moho jump

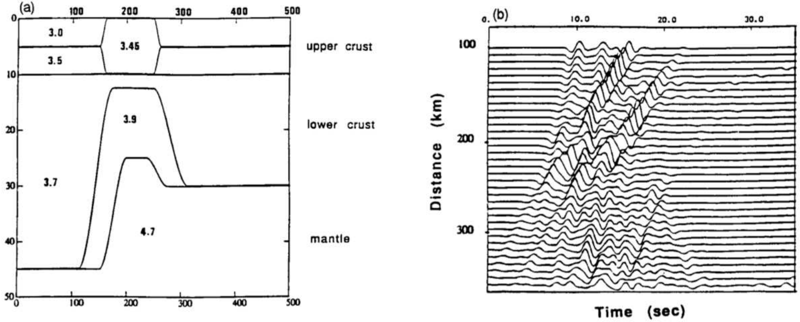

Chazalon et al. *GJI* 1993

Large Scale Structure

Conclusion

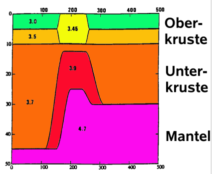

Even a very realistic macroscopic velocity structure is unable to explain the observed extent of Lg-wave attenuation. No geometrical effect. (Chazalon et al. *Geophys, J. Int.* 1993)

Small Scale Heterogeneity

Hypothesis

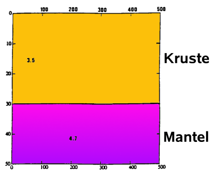

Small Scale Heterogeneity

Hypothesis

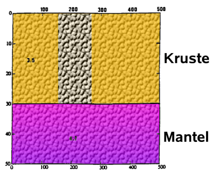

The blockage of Lg-waves is caused by scattering at small scale heterogeneity beneath the western Pyrenees.

Contents

Fundamentals of Radiative Transfer Theory

Basic quantity of RTT is the specific intensity $I(\omega, t, \mathbf{n}, \mathbf{r})$
$\Rightarrow$ frequency, time, space, and direction dependent Energy flux density

- describes the spatio–temporal distribution of seismic energy

Fundamentals of Radiative Transfer Theory

Basic quantity of RTT is the specific intensity $I(\omega, t, \mathbf{n}, \mathbf{r})$
$\Rightarrow$ frequency, time, space, and direction dependent Energy flux density

- describes the spatio–temporal distribution of seismic energy

$\Rightarrow$ model seismogram envelopes

Fundamentals of Radiative Transfer Theory

Basic quantity of RTT is the specific intensity $I(\omega, t, \mathbf{n}, \mathbf{r})$
$\Rightarrow$ frequency, time, space, and direction dependent Energy flux density

- describes the spatio–temporal distribution of seismic energy

$\Rightarrow$ model seismogram envelopes

- neglects wave phenomena (interference)

Fundamentals of Radiative Transfer Theory

Basic quantity of RTT is the specific intensity $I(\omega, t, \mathbf{n}, \mathbf{r})$
$\Rightarrow$ frequency, time, space, and direction dependent Energy flux density

- describes the spatio–temporal distribution of seismic energy

$\Rightarrow$ model seismogram envelopes

- neglects wave phenomena (interference)
- assumes a statistical distribution of heterogeneity

Fundamentals of Radiative Transfer Theory

Basic quantity of RTT is the specific intensity $I(\omega, t, \mathbf{n}, \mathbf{r})$
$\Rightarrow$ frequency, time, space, and direction dependent Energy flux density

- describes the spatio–temporal distribution of seismic energy

$\Rightarrow$ model seismogram envelopes

- neglects wave phenomena (interference)
- assumes a statistical distribution of heterogeneity
- may be based on an energy balance consideration

Energy Transfer Equation (acoustic case)

Change of intensity $I(\mathbf{n}, \mathbf{r})$ along a path element ds

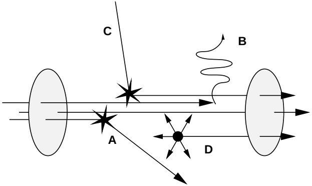

A decrease due to scattering (g_0)

B decrease due to absorption (b)

C increase due to sacttering ($g(\mathbf{n}, \mathbf{n}')$)

D increase due to sources

$$\frac{\partial}{\partial s} I(\mathbf{n}, \mathbf{r}) = -(g_0 + b) I(\mathbf{n}, \mathbf{r}) + \int_{4\pi} g(\mathbf{n}, \mathbf{n}') I(\mathbf{n}', \mathbf{r}) d\Omega_{\mathbf{n}'}$$

Elastic case

1 P-mode and 2 degenerate S-modes

- modes are coupled by conversion scattering coefficients g^{PS}, g^{SP} and g^{SS}
- S-wave scattering requires the treatment of polarization

Monte-Carlo technique to solve the RTE

- discretize the wave and propagate the wave packets independently like particles
- Intensity is modeled as the *number density* of these particles
- Movement of particles is governed by the large scale velocity structure (ray tracing)
- Interaction with medium small scale velocity structure (heterogeneity) by isolated scattering events

$\Leftarrow$ Probabilities for mode conversion and scattering angles are described by the scattering coefficients $g(\mathbf{n}, \mathbf{n}')$ from the Born-approximation

- (two S-polarizations are regarded as separate modes)

Characterization of the medium

- Medium has random velocity fluctuations:

$$v(r) = v_0(1 + \xi(r)) \quad \text{with} \quad \langle \xi(r) \rangle = 0 \quad \text{and} \quad \langle \xi(r)^2 \rangle = \varepsilon^2$$

- $\xi(r)$ is characterized by it's spectral density PSD (exponential ACF)

$$PSD(m) = \frac{8\pi\varepsilon^2 a^2}{(1 + a^2 m^2)^2}$$

with the correlation length a.

- The PSD enters the scattering coefficient g

$$g^{PP}(\Theta) = \frac{l^4}{4\pi} |X^{PP}(\Theta)|^2 PSD\left(\frac{2l}{\gamma_0} \sin\left(\frac{\Theta}{2}\right)\right)$$

Type and amplitude of velocity fluctuation governs the scattering process.

Elastic case – Treatment of the S-Polarisation

- assume linearly polarized waves

⇒ dependence of scattering coefficient on scattering angle Θ and Φ factorizes (great advantage for modeling)

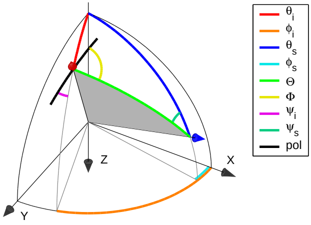

Elastic case – Treatment of the S-Polarisation

- assume linearly polarized waves

⇒ dependence of scattering coefficient on scattering angle Θ and Φ factorizes (great advantage for modeling)

- decompose arbitrary polarization into I_ϕ and I_θ

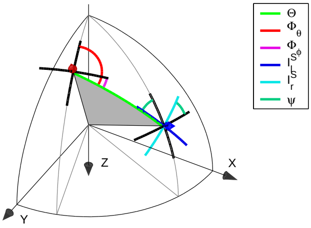

Elastic case – Treatment of the S-Polarisation

- assume linearly polarized waves

⇒ dependence of scattering coefficient on scattering angle Θ and Φ factorizes (great advantage for modeling)

- decompose arbitrary polarization into I_ϕ and I_θ

⇒ I_ϕ and I_θ propagate independently

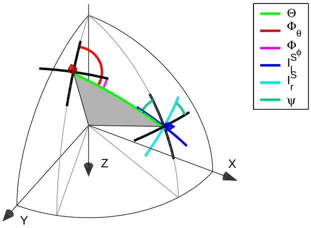

Elastic case – Treatment of the S-Polarisation

- assume linearly polarized waves

⇒ dependence of scattering coefficient on scattering angle Θ and Φ factorizes (great advantage for modeling)

- decompose arbitrary polarization into I_ϕ and I_θ

⇒ I_ϕ and I_θ propagate independently

⇒ three coupled RTEs for two S- and one P-mode

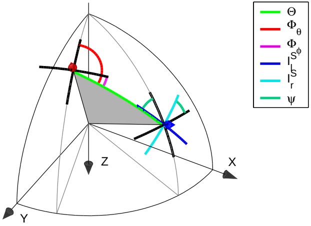

Monte-Carlo Simulation

Energy propagation in continental crust

- 30 km thick crust (constant velocity, strong scattering)
- mantle (velocity gradient, weak scattering)

\+ Interfaces

Monte-Carlo Simulation

Energy propagation in continental crust

- 30 km thick crust (constant velocity, strong scattering)
- mantle (velocity gradient, weak scattering)

+ Interfaces

Resulting phases in this model

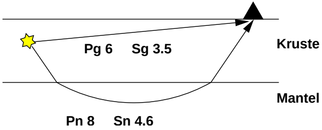

Pn - Pg - Sn - Sg

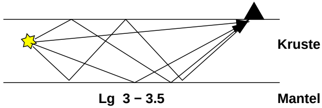

Lg: guided S-wave

Energy Propagation in the Model

Example

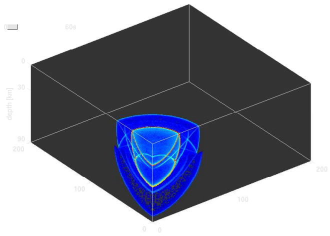

Contents

3D model of the locally increased heterogeneity

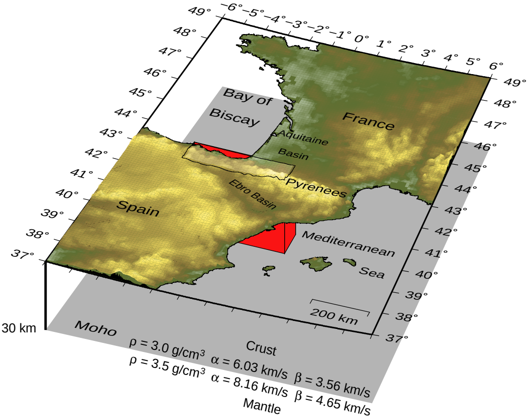

Inversion

Measurements

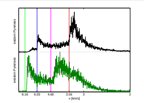

two reference envelopes for propagation through

- eastern Pyrenees (without obstacle)
- western Pyrenees (with obstacle)

Inversion

Model

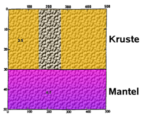

three blocks described by:

- intrinsic attenuation (Q)
- scattering strength l^*

Inversion

genetic algorithm

- random generation of starting models in $0.003 < \varepsilon < 0.3$, $0.1 < a < 100$ km, and $50 < Q^P < 5000$
- recombination of the parameters of successful models
- modification of individual parameters (mutation) with an exponentially distributed factor

$\Rightarrow$ random sampling of the parameter space

Results

Fit of data by predictions of the best model

eastern Pyrenees

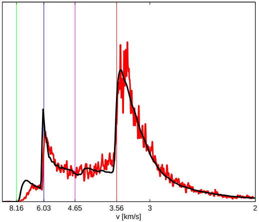

	${}^{I}Q^{P}$	${}^{I}Q^{S}$	ε	a	l_S^*
crust	1400	623	2.1%	0.77 km	750 km
mantle	1070	475	2.0%	2.0 km	1530 km

Results

Fit of data by predictions of the best model

western Pyrenees

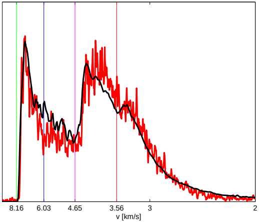

	$^{I}Q^{P}$	$^{I}Q^{S}$	ε	a	l_S^*
crust	1400	623	2.1%	0.77 km	750 km
mantle	1070	475	2.0%	2.0 km	1530 km
Pyrenean body	402	179	7.2%	0.77 km	63 km

Results

Intrinsic attenuation or scattering in the Pyrenees?

only increased intrinsic attenuation

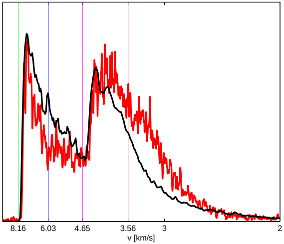

Results

Intrinsic attenuation or scattering in the Pyrenees?

only increased intrinsic attenuation

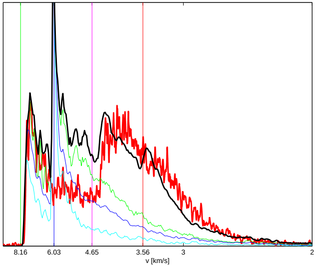

Results

Intrinsic attenuation or scattering in the Pyrenees?

only increased intrinsic attenuation

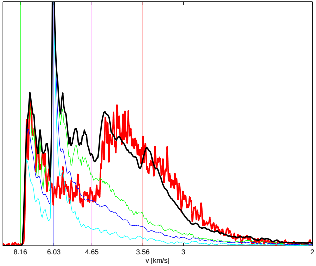

only increased scattering

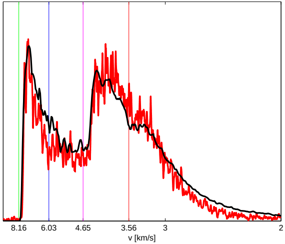

Results

Intrinsic attenuation or scattering in the Pyrenees?

only increased intrinsic attenuation

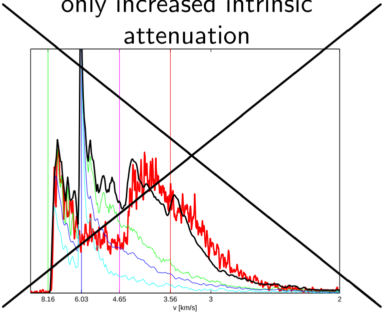

only increased scattering

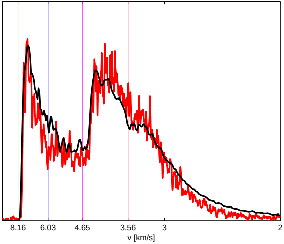

Results

spatial energy distribution

105 s lapse time

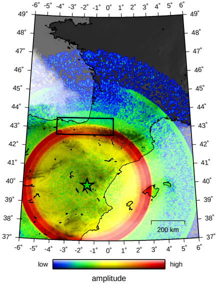

180 s lapse time

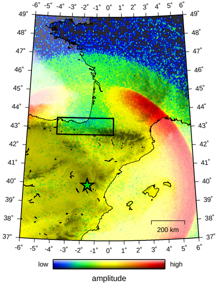

Interpretation

Effect of the continent-continent collision

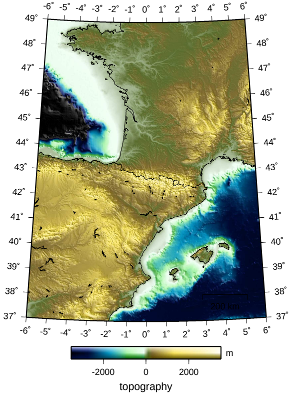

- eastern Pyrenees: convergent motion led to subduction of Iberian lower crust
- western Pyrenees: no subduction

Convergent and rotational motion led to strong internal deformation with exchange of material between different crustal layers. This heterogeneity causes the increased scattering that is responsible for the Lg-blockage.

Summary

- developed an algorithm for Monte-Carlo simulations of energy propagation
  - multiple elastic conversion scattering
  - combination of deterministically described large scale velocity structure and statistically described heterogeneity

Summary

- developed an algorithm for Monte-Carlo simulations of energy propagation
    - multiple elastic conversion scattering
    - combination of deterministically described large scale velocity structure and statistically described heterogeneity
- presented a detailed analysis of energy propagation through the Pyrenees

Summary

- developed an algorithm for Monte-Carlo simulations of energy propagation
  - multiple elastic conversion scattering
  - combination of deterministically described large scale velocity structure and statistically described heterogeneity
- presented a detailed analysis of energy propagation through the Pyrenees
- presented a model for the Lg-blockage in the western Pyrenees that explains the observation

Summary

- developed an algorithm for Monte-Carlo simulations of energy propagation
  - multiple elastic conversion scattering
  - combination of deterministically described large scale velocity structure and statistically described heterogeneity
- presented a detailed analysis of energy propagation through the Pyrenees
- presented a model for the Lg-blockage in the western Pyrenees that explains the observation
- showed that scattering is an important process for the Lg-blockage

References

Campillo, M., Feigner, B., Bouchon, M., and Bethoux, N. (1993). Attenuation of crustal waves across the Alpine range. *J. Geophys. Res.*, 98(B2):1987–1996.

Chazalon, A., Campillo, M., Gibson, R., and Carreno, E. (1993). Crustal wave propagation anomaly across the pyrenean range. comparison between observations and numerical simulations. *Geophys. J. Int.*, 115:829–838.

Przybilla, J., Korn, M., and Wegler, U. (2006). Radiative transfer of elastic waves versus finite difference simulations in two-dimensional random media. *J. Geophys. Res.*, 111(B10):4305–+.

Acknowledgements

We like to thank

- CEA/DASE for providing the data for this study
- DFG (grant WE 27213), DAAD, EU (NERIES), LGIT for financial support

Laterally heterogeneous scattering explains Lg blockage in the Pyrenees, C. Sens-Schönfelder, L. Margerin, M. Campillo, *Journal of Geophysical Research*, Vol.114, B07309, 2009